EARTH OBSERVATION AND GEOMATICS ENGINEERING
website: https://eoge.ut.ac.ir

Bridge Vertical Deformation Monitoring Using GBSAR Repeat-Pass Observations

Benyamin Hosseiny[1], Jalal Amini[1]*

[1]School of Surveying and Geospatial Engineering, College of Engineering, University of Tehran, Tehran, Iran

Article history:
Received: 2023-03-17, Accepted: 2023-05-01, Published: 2023-06-14

ABSTRACT

This study presents the feasibility and performance evaluation of a developed ground-based synthetic aperture radar (GBSAR) system for monitoring vertical displacement in bridge structures. Bridges, as critical transportation infrastructures, require regular assessment to ensure safety. In recent years, ground-based radar and synthetic aperture radar (SAR) systems have demonstrated their effectiveness as non-contact displacement monitoring tools for structural displacement monitoring. This study utilizes a prototype GBSAR system consisting of a W-band radar, TI-AWR1642BOOST, with a maximum signal bandwidth of 4 GHz, incorporated with a 15 cm horizontal mechanical rail to enhance cross-range resolution. To evaluate the performance of the GBSAR, two types of experiments were conducted: laboratory experiments in a controlled situation and outdoor simulations by creating a light-weight bridge and inducing displacements through the addition or removal of loads on its surface. The results obtained from the laboratory experiments showcased a measurement accuracy ranging from 50 to 80 micrometers in vertical displacement, while the results from the simulated bridge showed a final accumulated vertical displacement error below 1 mm. These overall results validate the applicability of the developed GBSAR system for vertical displacement monitoring of structures with sub-millimeter accuracy.

KEYWORDS

Radar remote sensing, ground-based synthetic aperture radar, terrestrial radar interferometry, InSAR, Structural health monitoring

1. Introduction

The measurement and monitoring of structural displacement play a crucial role in the field of structural health monitoring (SHM), especially for critical transportation infrastructures such as bridges, where regular assessments are necessary to ensure safe operation. One specific aspect of these assessments involves tracking the behavior of bridges over time, as any changes in behavior may indicate damage or deterioration within the structure. Typically, observed properties include displacement and frequency parameters of the vibrations that occur after applying a load to the bridge deck. These parameters can be influenced by external factors, including applied force and temperature variations within the structure. Therefore, obtaining a reliable estimation of the bridge's properties requires a significant number of measurements taken under various load and weather conditions (Michel & Keller, 2021). In recent years, several approaches based on contact and non-contact methods have been developed to address this need. Contact sensors, such as accelerometers and strain gauges, can be installed on structures to accurately measure displacements and vibrations (Omidalizarandi et al., 2018; Sabato et al., 2017) . However, their usage may prove

* Corresponding author

E-mail addresses: ben.hosseiny@ut.ac.ir (B.Hosseiny); jamini@ut.ac.ir (J.Amini)

challenging, risky, or even impossible depending on the nature of the monitored object (Michel & Keller, 2021). In contrast, non-contact systems, such as optical sensors like vision-based sensors, total stations, and laser scanners, allow for monitoring of displacements without physically connecting to the infrastructure (Mugnai et al., 2022). Nevertheless, optical sensors are susceptible to environmental conditions such as fog and rain (C. Li et al., 2015; Wu & Casciati, 2014). Radar remote sensing offers an alternative non-contact method that can overcome the aforementioned limitations.

Radar has demonstrated remarkable insensitivity to environmental conditions, while providing high-resolution, precise, and frequent data, making it an ideal technology for SHM. Radar data is typically divided into amplitude and phase components, with the amplitude providing information about physical properties and the phase relating to the range of the monitored scene. The sensitivity of radar's phase to target range has led to the development of techniques that derive target movement or height information by analyzing the interference of at least two phase measurements. The primary application of radar interferometry in remote sensing applications is surface and structural displacement monitoring. Additionally, synthetic aperture radar (SAR) imaging has enabled high-resolution radar imaging by coherently integrating received signals from different locations along the radar's path (Carrara et al., 1995). Radar sensors can be deployed on spaceborne, airborne, or ground-based platforms. Space-based radar techniques allow for displacement monitoring with sub-millimeter accuracy (Bamler & Hartl, 1998; Pepe & Calò, 2017; Radman et al., 2021). Multi-baseline and/or time-series SAR, which involves processing radar signals acquired at different cross-range locations, provides cross-range resolution (Reigber et al., 2013). Radar interferometry forms the basis for multidimensional radar imaging and displacement monitoring (Aghababaei, 2020; Rambour et al., 2020). Satellite-based SAR interferometry (InSAR) is a well-established tool for large-scale environmental monitoring of the Earth. On the other hand, terrestrial (or ground-based) radar interferometry (TRI), ground-based SAR (GBSAR) interferometry (GBInSAR), and more recently, ground-based multiple input multiple output (MIMO) radars are considered non-contact systems that offer better temporal resolution and lower atmospheric impact compared to satellite data, making them suitable for monitoring dynamics in small areas (Akbari et al., 2018; W. Li et al., 2020; Zhang et al., 2020).

Ground-based radar systems are capable of mitigating or minimizing the significant limitations associated with satellite radar observations. These limitations include infrequent data acquisition, usually occurring once every few days, suboptimal viewing angles in comparison to the desired observation range, coarse spatial resolution, and atmospheric error effects. Ground-based radar systems commonly utilize frequency modulated continuous wave (FMCW) signals, in which the transmitted signal frequency continuously changes over time, resulting in improved range resolution. The utilization of FMCW signals reduces the requirement for high transmit power, thereby leading to lower costs and smaller system dimensions (Charvat, 2014; Komarov & Smolskiy, 2003). Another advantage offered by ground-based radar is its ability to acquire data at a high rate. In particular, a real-aperture ground-based radar (GBRAR) can obtain data within fractions of a second, while in synthetic aperture mode (GBSAR), data acquisition can be completed in less than a few minutes. Consequently, when compared to satellite modes, the high temporal resolution of ground-based radars enables rapid monitoring of fast-moving targets for early warning systems, as well as minimizes phase ambiguity and errors induced by atmospheric conditions.

GBSAR systems typically achieve cross-range resolution by moving the radar sensor along a mechanical rail in a specified trajectory (Monserrat et al., 2014). The first GBSAR system, known as Linear SAR (LISA), was introduced by Tarchi et al., (2000) and used for structural displacement monitoring. Since then, various types of GBSAR systems with two-dimensional linear (Hosseiny, Amini, & Aghababaei, 2023) or arc-shaped (Luo et al., 2014) synthetic apertures, MIMO (Mugnai & Tarchi, 2022), multi-static (Miccinesi & Pieraccini, 2020), or distributed ground-based radars (Monti-Guarnieri et al., 2018) have been introduced in this field. Currently, ground-based systems used to monitor civil structures primarily operate in higher frequency bands such as Ku, Ka or even W bands. These frequency bands provide high spatial and temporal resolution data, allowing for the detection of small deformations with sub-millimeter accuracy. Moreover, operating at higher frequencies, such as the millimeter-wavelength W band (77 GHz), allows for more compact and lighter system designs, making deployment easier.

However, W-band radars have weaker signal power due to their shorter wavelength and are more sensitive to atmospheric conditions compared to lower frequencies. As a result, they are best suited for monitoring individual objects like buildings, bridges, pipelines or wind turbines (Baumann-Ouyang et al., 2023; Guarnieri et al., 2022; Hosseiny, Amini, Aghababaei, et al., 2023; Miccinesi et al., 2021a). Automotive W-band radars are currently popular options due to their low cost and availability in the market. These radars utilize MIMO technology, which enables angular resolution by employing multiple transmitter and receiver antennas in a non-Nyquist geometry. Several recent studies have shown the effectiveness of W-band MIMO radars for structural monitoring with nominal precision typically better than 0.1 mm per observation (Ciattaglia et al., 2020; GAMBI et al., 2019; Hosseiny et al., 2021). Baumann-Ouyang et al., (2021) evaluated the capabilities of a MIMO radar, called TIDEP-01012 from Texas Instruments (TI), for structural monitoring in various weather conditions. Miccinesi et al., (2021) designed a compact GBSAR using a MIMO radar and a mechanical rail. These studies demonstrate the significant potential of

these kinds of ground-based radars as suitable tools for geodetic monitoring of small areas with high precision and resolution, while, as said earlier, having various advantages compared to the conventional sensors such as GNSS receivers or total stations.

By showcasing the effectiveness of GBSAR systems in displacement monitoring, as well as highlighting the high potential of W-band radars for short-range structural displacement monitoring in the literature review, the primary objective of this paper is to assess the performance of a developed W-band GBSAR system for monitoring vertical displacement in bridges. The developed GBSAR utilizes a horizontal mechanical rail to generate a high-resolution synthetic aperture, and incorporates the AWR1642BOOST W-band radar sensor manufactured by TI. To validate the capabilities of the developed system, both laboratory and outdoor experiments were conducted, and the obtained results were thoroughly discussed.

The rest of the paper is organized as follows. Section 2 provides the materials and method of this study including the details of the developed GBSAR system and the proposed processing chain. The experimental results of laboratory and outdoor experiments are detailed in Section 3. Finally, the concluding marks are drawn in Section 4.

2. Material and Method

This section demonstrates the developed GBSAR prototype and the implemented approach for monitoring the bridge vertical displacements from the GBSAR's repeat-pass observations. Figure 1 shows the geometry between the GBSAR and the monitored bridge. A GBSAR collects data along its range and cross-range directions. Thus, one GBSAR acquisition results in a complex-valued two-dimensional matrix namely single look complex (SLC) image. Each complex-valued pixel contains the amplitude and phase of the backscattered radar echo from the surface located at the radar's range and cross-range. Radar can measure the displacement acquired at each resolution bin by differentiating the phase values of the corresponding pixels acquired at different times, which is also called differential interferometry. The measured displacement is along the radar's LOS.

In order to obtain the vertical displacement, one must collect SAR data from various locations using at least three SAR sensors (C. Li et al., 2015) or possess prior knowledge of the monitoring scene. Notably, in the first case, the 3D displacement vector can be estimated from the LOS observations. This prior knowledge can include having a digital elevation model or understanding the relative geometry between the radar antenna and the object, such as their height difference (Michel & Keller, 2021). The latter case, which is more common in short-range ground-based

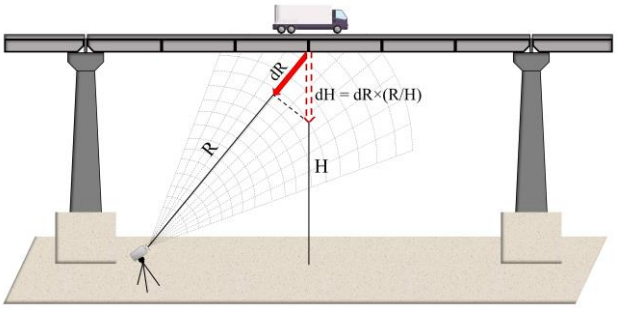

Figure 1. measurement geometry of GBSAR and the relation between the actual vertical displacement (dH) and the measure LOS displacement (dR)

radar and SAR, requires the projection of the measured LOS displacement into the vertical axis. This projection can be achieved by knowing the height difference between the GBSAR and the point of interest on the bridge

$$dH = dR(\frac{R}{H}) \quad (1)$$

where dH and dR are the displacement in vertical and LOS directions, while H and R are the scatterer's distance from the GBSAR sensor in vertical and slant range directions, respectively.

2.1. GBSAR System

The developed GBSAR consists of a radar sensor, data acquisition board, a horizontal linear stepper, and a personal computer (PC). The utilized radar instrument is AWR1642BOOST[1], manufactured by Texas Instruments (TI). It consists of 4 receivers and 2 transmitter antennas in MIMO geometry. The operating signal is linear frequency modulated continuous wave (FMCW) in the frequency range of 76-81 GHz in W band, yielding a wavelength of approximately 3.8 millimeters. The maximum dedicated signal bandwidth is 4 GHz, providing a maximum of 4 cm resolution in range direction.

After the dechirping process, which includes mixing with a reference signal and low-pass filtering, the DCA1000EVM module by TI sends the digitized captured data to the PC through Ethernet. In order to form a synthetic aperture radar (SAR) signal acquisition mode, the radar sensor is mounted on a horizontal linear rail. This leads to a higher cross-range resolution after processing the acquired signals. The linear rail is attached to a stepper motor, where enforces the rail's rotation in forward or backward directions. Before starting the data acquisitions, the user defines the sensor's movement behavior, including the trajectory and velocity. These parameters are programmed through an Arduino microcontroller chip, which is connected to the stepper motor. Furthermore, the user has the ability to set the signal transmission parameters, such as the number of chirps, their duration, and repetition time. This information allows for the

[1] https://www.ti.com/product/AWR1642

precise location of each signal during data collection, which in turn enables the generation of a time-series raw data cube for processing. The maximum length of the utilized mechanical rail is 15 cm, while the rail's rotation velocity is up to 5 mm/s. The mentioned system parameters are summarized in Table 1.

Table 1. Parameters of the system used in this study

Name	**Value**
Radar model	TI-AWR1642BOOST
Signal type	Linear FMCW
System's operating frequency	76-81 GHz
Carrier frequency (f_c)	77 GHz
Wavelength (λ)	0.0038 m
bandwidth (B)	Up to 4 GHz
Range resolution	Up to 0.04 m
Range samples	512
Sweep time	60 μs
Maximum length of SAR	0.15 m
Maximum cross-range resolution	0.013 rad
SAR velocity	0.005 m/s

Figure 2 shows the data acquisition work flow in order to capture structural displacements through GBSAR signal. In order to obtain the suitable data from the monitoring area it is required to set the optimum parameters before starting the data acquisition. Thus, the main steps for data acquisition can be summarized as follows:

1- Setting up the developed Matlab toolbox, which is integrated with the radar sensor's built-in software (mmWave studio by TI).

2- Configuring the system parameters such as carrier frequency, bandwidth, chirp duration, and periodicity.

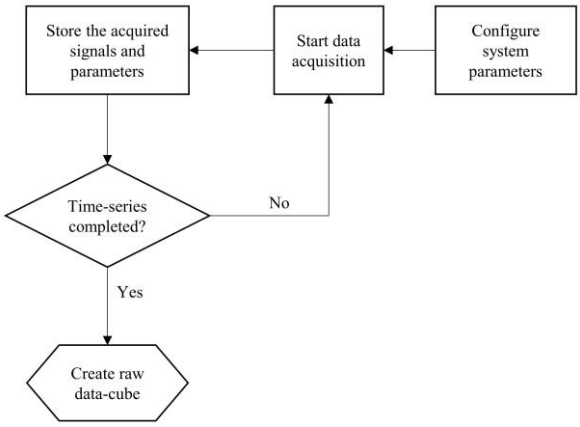

Figure 2. Time-series repeat-pass data acquisition process of the developed GBSAR

3- Starting the data collection by moving the radar sensor along the rail on the given trajectory.

4- Preparing the raw data-cube from the collected signals and storing it and system parameters in the hard drive.

5- Repeating steps 3 and 4 until collecting the desired tracks of time-series data.

6- Creating the time-series data cube by stacking the acquired signals in different passes. This results in a 3D matrix with the size of $N_r \times N_{az} \times N_q$, where N_r, N_a, and N_q represent the number of samples in the directions of fast time (range) denoted by r, slow time (azimuth) denoted by a, and repeat time (time) denoted by q.

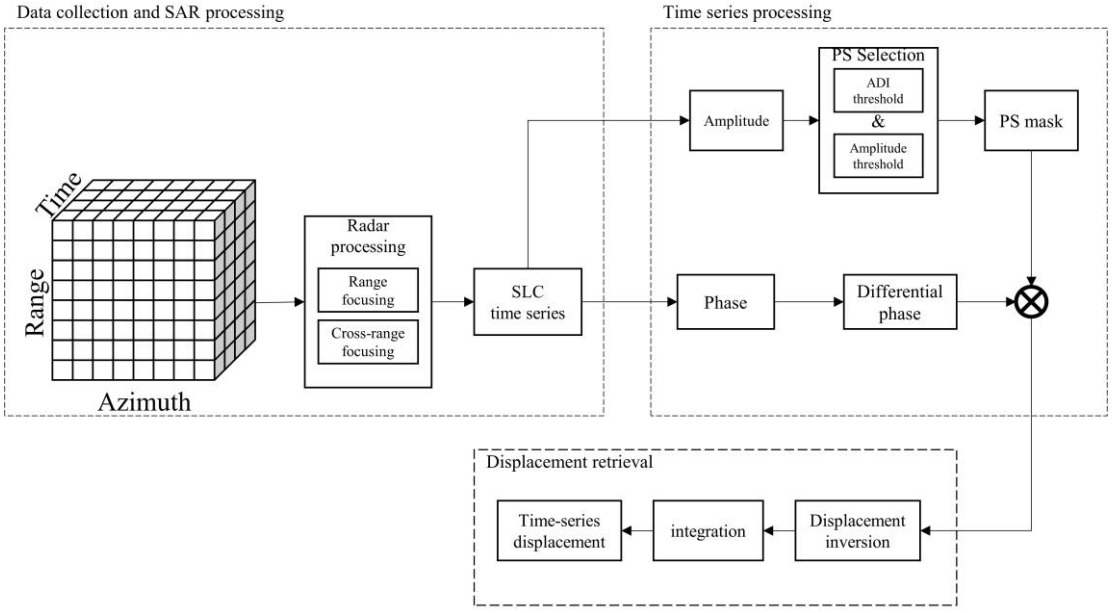

Figure 3. the utilized processing flow for retrieving displacement maps from GBSAR time-series observations

2.2. Data acquisition and Processing flow

Persistent scatterer interferometry (PSI) is utilized in this study order to retrieve displacement signal from the collected repeat-pass GBSAR data.

Figure 3 demonstrates the steps of the implemented processing flow for displacement retrieval from a time series of GBSAR data and PSI algorithm (Wang et al., 2020).

After the receiver antennas collect the backscattered echoes, and performing dechirping process the received intermediate frequency signal from the m^{th} virtual antenna of GBSAR is as follows:

$$s_{if}(m,t) = \exp\left\{ j2\pi \left(f_0\tau + k_r\tau t - \frac{k_r\tau^2}{2} + \frac{2ml\sin\theta}{\lambda} \right) \right\} \quad (2)$$

where $s_{if}(m,t)$ is the received intermediate frequency signal to the m^{th} antenna, k_r is chirp slope, f_0 is signal's starting frequency, λ is wavelength, τ is scattering target's time delay, θ is scattering target's cross-range angle, l is the step size between two radar acquisitions in cross-range direction during SAR imaging. After collecting a time-series of repeat-pass GBSAR signals, the raw data cube forms a 3D $N_r \times N_a \times N_q$ matrix.

The focused signal in range and cross-range directions can be achieved by Fourier transformation of raw signals at each direction. Thus, a complex-valued radar image is obtained in radar's polar coordinate system, where the axes are slant range (R), cross-range angle (θ). In this case, following transformation is required to transform the obtained image into Cartesian coordinate system:

$$\begin{cases} X = R.\sin\theta \\ Y = R.\cos\theta \end{cases} \quad (3)$$

where (X,Y) is the Cartesian coordinate of a point target located at (R,θ) in the Polar coordinate system.

Each pixel of the resulting radar image consists of a complex number comprising the phase and amplitude. The amplitude corresponds to the scattering power of the pixel and can be used to interpret the image scene. Meanwhile, the phase contains range information and is used to measure deformation.

Reliable pixels are chosen based on the amplitude information of the collected time series of MIMO radar images by generating PS mask using the following criteria:

$$\begin{cases} \mu_A > -20\,dB \\ \rho_A = \dfrac{\sigma_A}{\mu_A} < 0.1 \end{cases} \quad (4)$$

where μ_A and σ_A are a spatial pixel's average amplitude and standard deviation in time, and ρ_A is the amplitude dispersion index, which evaluates pixels' stability during time. Thus, unreliable pixels are filtered out by element-wise multiplication of PS mask and the acquired time series of SLC images.

Radar's LOS displacement can be measured based on the phase difference that occurs between two observations at two different times. Therefore, the corresponding LOS displacement of a detected PS pixel is measured in two

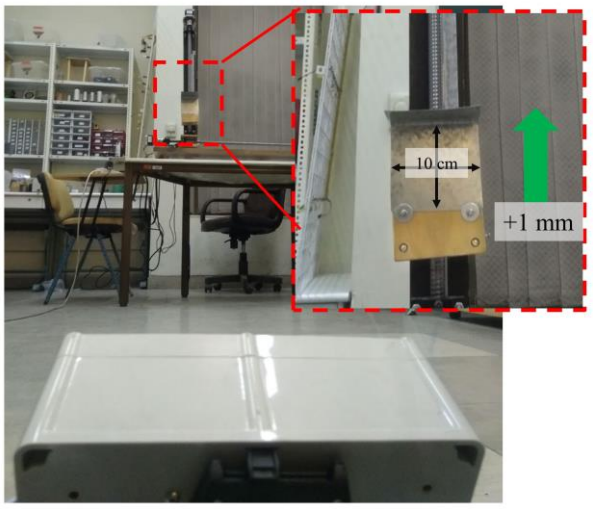

Figure 4. the laboratory experiment setup: a 10 cm dihedral metallic corner reflector is located at the horizontal and vertical distances of 2.5 m and 1.16 m from the GBSAR, where at each epoch of observation the CR is moved 0.001 m in the upward direction by a mechanical rail

epochs of t_1 and t_2

$$\Delta R(t_1,t_2) = \frac{\lambda}{4\pi}\Omega(\psi_2 - \psi_1) \quad (5)$$

where $\Delta R(t_1,t_2)$ is the measured displacement between two epochs of t_1 and t_2, and ψ_1 and ψ_2 are the measured radar phases of the target in the corresponding times. Ω is the wrapping operator that returns the phase value in the range of $[-\pi,\pi]$. Target's displacement at time t_N with respect to the first observation can be achieved by the summation of differential displacements from t_0 to t_N. Thus, a PS pixel's deformation signal in time is as follows

$$\Delta R(n) = \sum_{i=0}^{n-1} \Delta R(t_i, t_{i+1}) \quad (6)$$

3. Experimental results

This section presents the results of experiments on monitoring structural vertical displacement using a GBSAR sensor. Firstly, laboratory experiments were conducted within a controlled environment in order to validate the accuracy and correctness of the implemented methodology. Following that, a simulated scenario of bridge monitoring was utilized in order to demonstrate the practicality and effectiveness of the method in real-world situations.

3.1. Laboratory tests

The laboratory tests involved mounting a 10 cm metallic corner reflector in the shape of a dihedral on a vertical translational stage. The experimental setup, depicting the placement of the corner reflector and GBSAR sensor, is illustrated in Figure 4. The corner reflector was positioned

at a height of 1.16 m and a horizontal distance of 2.5 m from the GBSAR, resulting in a radar LOS range of 2.76 m.

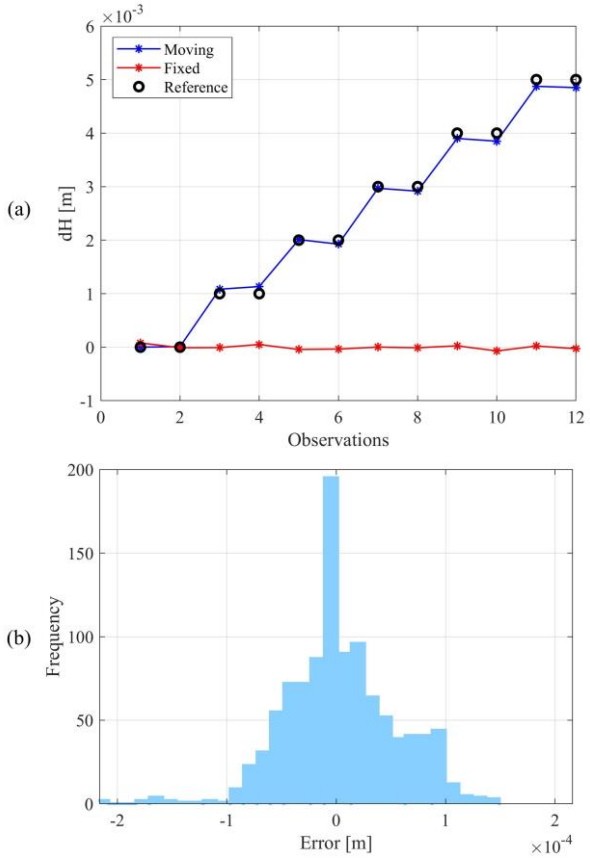

Figure 7. Obtained results for laboratory experiments: a) the cumulative displacement profiles of fixed points and CR, in comparison to the reference values, b) error distribution of observations

During the experiment, each time that the corner reflector was moved 1 mm in the upward direction, two SAR data were acquired by the GBSAR. The radar sensor's maximum obtainable bandwidth of 4 GHz was utilized in this study, resulting in a range resolution of 4 cm. Additionally, a synthetic aperture length of 10 cm was considered, which provided an angular resolution of 0.02 radians in the cross-range direction. Each data acquisition process took approximately one minute. Throughout the experiment, a total of 12 epochs of repeat-pass data were collected during the 5 upward steps of the corner reflector.

After performing interferometric processing on the collected time-series data, each LOS displacement signal was projected onto the vertical axis to determine the vertical displacement. The results of the laboratory experiments are presented in Figure 5. Figure 5-a illustrates the cumulative displacement pattern over time for the investigated corner reflector, comparing it with the reference values and the average displacement pattern of the fixed scatterers. It is evident from the figure that the measured displacements obtained through the interferometric processing of GBSAR time-series data closely align with the reference values. The estimated mean absolute error (MAE) between the measured and reference values for the vertical displacement of the moving scatterers is calculated to be 82 microns. On the other hand, the time-series displacement signal of the fixed scatterers remains close to zero throughout the measurement duration. Figure 5-b displays the distribution of measured displacements for the fixed points, which provides an estimation of the GBSAR's displacement measurement error. The distribution exhibits a Gaussian shape, with a mean value near zero and a standard deviation of 49 micrometers.

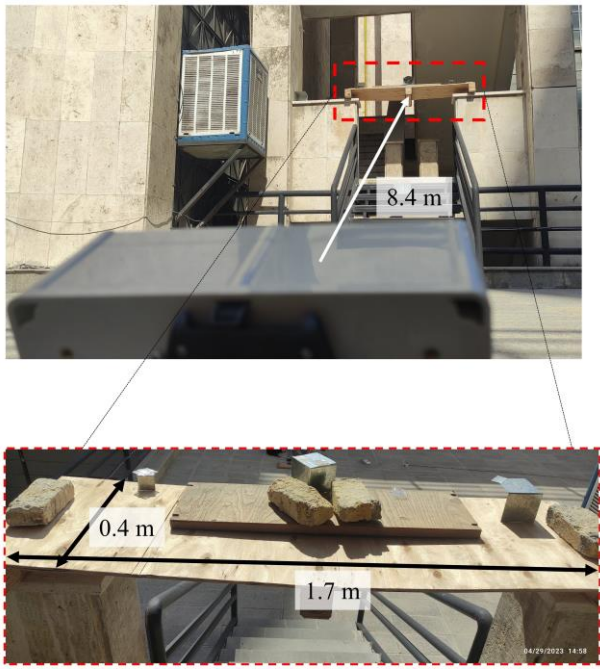

Figure 6. Study area containing a simulated wooden bridge with dynamic load. The GBSAR was located at the distance of about 8.4 m from the center of the bridge

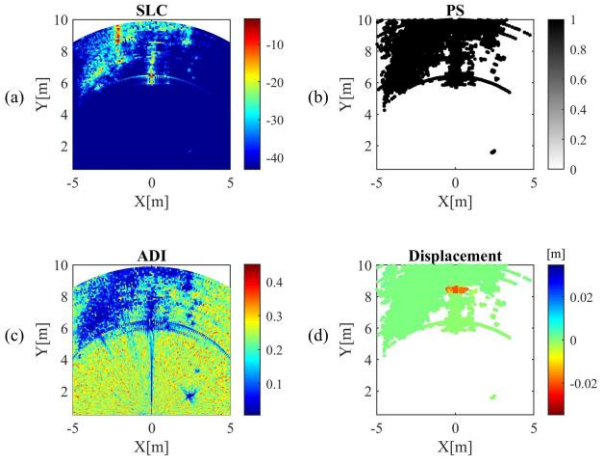

Figure 5. The processing results of the collected GBSAR data: a) SLC image of the scene from the first observation. b) PS mask. c) ADI image. d) Cumulated vertical displacement of the scene in the maximum displacement when all the loads were added on the bridge

3.2. Bridge tests

In order to conduct a more realistic experiment, we simulated a light-weight wooden bridge in an outdoor environment. Figure 6 illustrates the experimental area and the positioning of the bridge in relation to the GBSAR sensor's location. The bridge had a length of 1.7 m and a width of 0.4 m, secured between two concrete edges. Its center was situated at a height of 2.6 m, and it was located 7.99 m horizontally away from the GBSAR sensor, resulting in a radar LOS range of 8.4 m. To enhance the backscattering power from the bridge's surface, three trihedral metallic corner reflectors were affixed to its structure.

The bridge was subjected to displacement by manually adding or removing external loads. During the experiment, two SAR data sets were acquired by the GBSAR each time the load on the bridge was changed. In order to increase the maximum range of the recorded data, a signal bandwidth of 1.5 GHz was employed, resulting in a radar resolution of 10 cm in the range direction. Additionally, a synthetic aperture length of 10 cm was used, providing an angular resolution of 0.02 radians in the cross-range direction, consistent with the laboratory experiments. Throughout the experiment, a total of 22 epochs of repeat-pass data were collected, consisting of 5 downward steps achieved by adding loads to

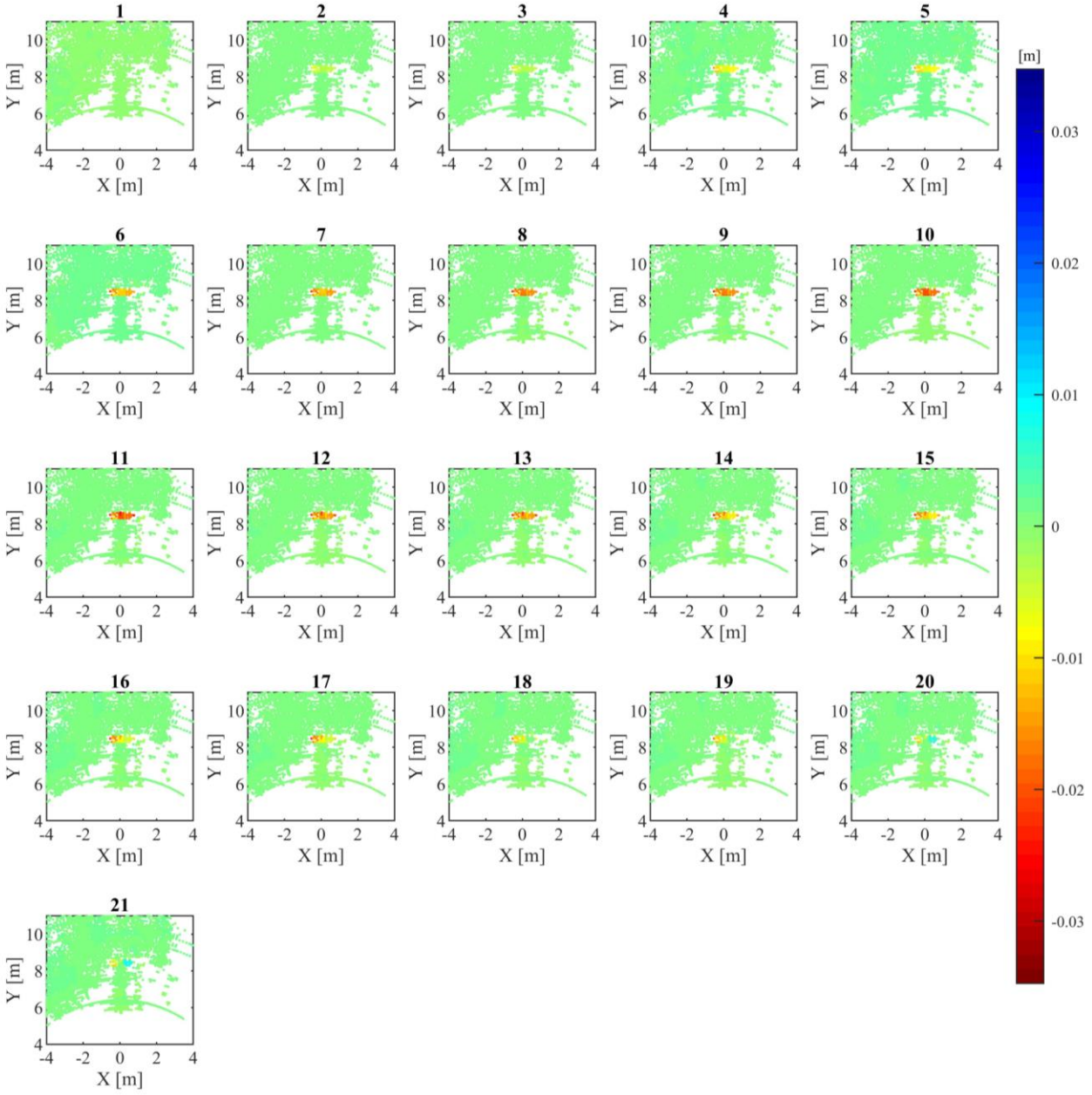

Figure 8. time-series cumulative vertical displacement maps obtained from InSAR processing of GBSAR data

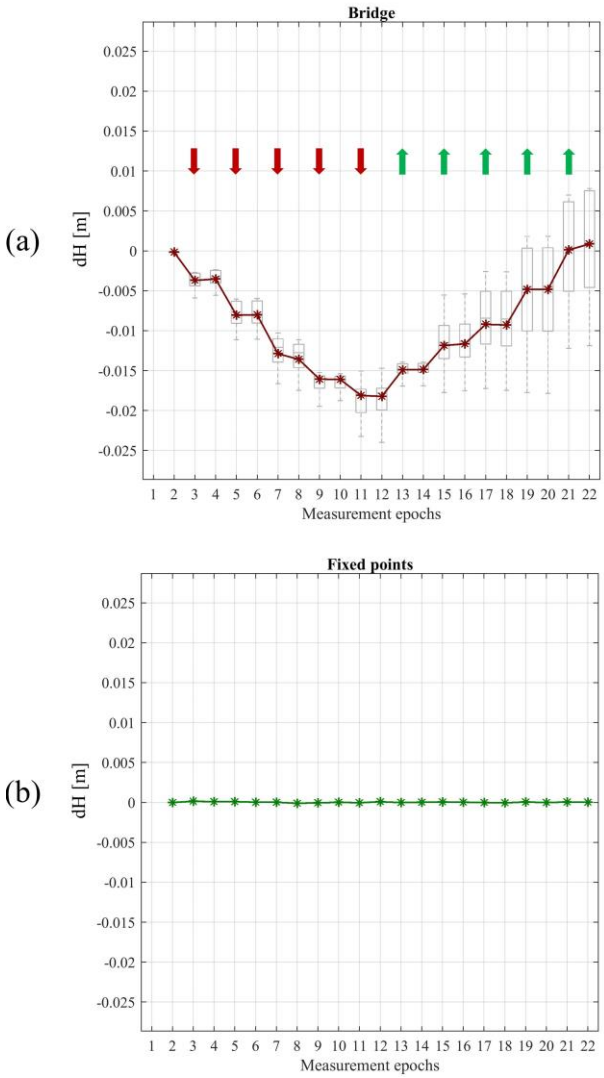

Figure 9. vertical displacement profiles: a) Displacement profile of scatterers detected on the bridge's area, b) Displacement profile of fixed scatterers in the background. (Red arrows represent the bridge's descending displacement by increasing the load, and green arrows represent the bridge's ascending displacement by decreasing the load)

the bridge, followed by 5 downward steps where the added loads were removed.

The collected time-series data was processed using the PSI method. Figure 7 illustrates the results obtained at each processing step, which include the SLC image, PS mask, ADI map, and the displacement map of the scene when subjected to maximum displacement caused by applying maximum load to the bridge. From the results, it can be observed that the bridge area does not exhibit strong backscattering power compared to its surroundings (Figure 7-a). Nevertheless, numerous stable scatterers with small ADI values were present in that area, while the precise location of the bridge can be found on the displacement map by showing a different displacement values compared to the fixed background.

Each LOS time-series displacement signal was projected onto the vertical axis to determine the vertical displacement. The obtained 21 vertical displacement maps at each time of observation are displayed in Figure 8, highlighting the stability of fixed background PS points with near-zero displacements. In contrast, the scatterers related to the bridge exhibit a distinctive displacement pattern, clearly differentiating the bridge area from the fixed background. The displacement maps over time clearly depict a downward and subsequent upward displacement in the bridge area.

The time-series cumulative vertical displacement pattern of the scatterers corresponding to the bridge and the fixed background is separately shown in Figure 9. The GBSAR measurements clearly indicate a pattern of downward and upward movement of the bridge, while the fixed points demonstrate near-zero displacement values, as expected. The measured displacement pattern of the bridge aligns with the times of adding or removing load from its surface. Notably, by having this knowledge that the bridge has returned to its initial position after removing all the loads, it is found that the average measured height difference between the first and last observations, both taken under the same situation without any external load, is less than 1 mm. However, it is worth noting that as we move along the observations, the displacement distribution of the scatterers corresponding to the bridge widens, indicating an increase in standard deviation and measurement error (see boxplots in Figure 9-a). This could be attributed to two possible reasons: error propagation through time-series observations or the simulated bridge's stability being compromised due to the additional load.

4. Conclusion

Bridges as critical transportation infrastructures require regular assessments to ensure safe operation. In recent years, ground-based radar and SAR systems have demonstrated their effectiveness as non-contact displacement monitoring systems in SHM. This study aimed to assess the feasibility and performance of a developed GBSAR system for monitoring vertical displacement in bridges. The developed prototype GBSAR consists of a W-band radar, TI-AWR1642BOOST, including a data acquisition board and maximum signal bandwidth of 4 GHz. To improve cross-range resolution, a horizontal mechanical rail with a length of 15 cm was incorporated into the system. Time-series data acquired through repeat-pass GBSAR observations were processed using PSI techniques to extract displacement signals along the LOS direction. These displacements were then projected onto the vertical axis, assuming one-dimensional displacement. To demonstrate the capabilities of the GBSAR system, two types of experiments were conducted. Firstly, a controlled laboratory scenario was employed, where a corner reflector was systematically displaced upward by 1 mm in the vertical axis after every two epochs of GBSAR observations. The results showcased a measurement accuracy ranging from 50 to 80 micrometers, highlighting the capability of the developed GBSAR to

detect small displacements accurately. In the second experiment, a light-weight wooden bridge was simulated in the outdoor environment. Dynamic loads were introduced or removed during data acquisition to induce bridge displacement. The results indicated a final accumulated displacement error of less than 1 mm. However, an increase in measurement error was observed when progressing through time-series observations, potentially due to error propagation or compromised stability of the simulated bridge caused by additional loads. Potential subjects for the future works can be analyzing the applicability of the developed GBSAR system in real-life case studies and exploring its potential for monitoring structural vibrations.

References

Aghababaei, H. (2020). On the assessment of non-local multi-looking in detection of persistent scatterers using SAR tomography. *Remote Sensing*, *12*(19), 3195.

Akbari, V., Lauknes, T. R., Rouyet, L., Negrel, J., & Eltoft, T. (2018). Validation of SAR iceberg detection with ground-based radar and GPS measurements. *International Geoscience and Remote Sensing Symposium (IGARSS)*, *2018-July*, 4623–4626. https://doi.org/10.1109/IGARSS.2018.8517286

Bamler, R., & Hartl, P. (1998). Synthetic aperture radar interferometry. *Inverse Problems*, *14*(4), R1.

Baumann-Ouyang, A., Butt, J. A., Salido-Monzú, D., & Wieser, A. (2021). MIMO-SAR Interferometric Measurements for Structural Monitoring: Accuracy and Limitations. *Remote Sensing 2021, Vol. 13, Page 4290*, *13*(21), 4290. https://doi.org/10.3390/RS13214290

Baumann-Ouyang, A., Butt, J. A., Varga, M., & Wieser, A. (2023). MIMO-SAR Interferometric Measurements for Wind Turbine Tower Deformation Monitoring. *Energies*, *16*(3), 1518.

Carrara, W. G., Goodman, R. S., & Majewski, R. M. (1995). *Spotlight synthetic aperture radar: Signal processing algorithms*. Artech House. https://searchworks.stanford.edu/view/3116166

Charvat, G. L. (2014). *Small and short-range radar systems*. CRC Press.

Ciattaglia, G., Santis, A. D., Disha, D., Spinsante, S., Castellini, P., & Gambi, E. (2020). Performance Evaluation of Vibrational Measurements through mmWave Automotive Radars. *Remote Sensing 2021, Vol. 13, Page 98*, *13*(1), 98. https://doi.org/10.3390/RS13010098

GAMBI, E., CIATTAGLIA, G., & SANTIS, A. D. (2019). AUTOMOTIVE RADAR APPLICATION FOR STRUCTURAL HEALTH MONITORING. *WIT Transactions on The Built Environment*, *189*, 79–89.

Guarnieri, A. M., Wang, J., Wang, Y., Li, Y., & Huang, X. (2022). Fast Displacement Estimation of Multiple Close Targets with MIMO Radar and MUSICAPES Method. *Remote Sensing 2022, Vol. 14, Page 2005*, *14*(9), 2005. https://doi.org/10.3390/RS14092005

Hosseiny, B., Amini, J., & Aghababaei, H. (2023). Structural displacement monitoring using ground-based synthetic aperture radar. *International Journal of Applied Earth Observation and Geoinformation*, *116*, 103144. https://doi.org/10.1016/j.jag.2022.103144

Hosseiny, B., Amini, J., Aghababaei, H., & Ferraioli, G. (2023). Enabling High-Resolution Micro-Vibration Detection Using Ground-Based Synthetic Aperture Radar: A Case Study for Pipeline Monitoring. *Remote Sensing*, *15*(16). https://doi.org/10.3390/rs15163981

Hosseiny, B., Amini, J., & Safavi-Naeini, S. (2021). Simulation and Evaluation of an mm-Wave MIMO Ground-Based SAR Imaging System for Displacement Monitoring. *2021 IEEE International Geoscience and Remote Sensing Symposium IGARSS*, 8213–8216. https://doi.org/10.1109/IGARSS47720.2021.9553347

Komarov, I. V, & Smolskiy, S. M. (2003). *Fundamentals of short-range FM radar*. Artech House.

Li, C., Chen, W., Liu, G., Yan, R., Xu, H., & Qi, Y. (2015). A noncontact FMCW radar sensor for displacement measurement in structural health monitoring. *Sensors*, *15*(4), 7412–7433.

Li, W., Wang, Z., Wang, Y., Wu, J., Wang, J., Jia, Y., & Gui, G. (2020). Classification of high-spatial-resolution remote sensing scenes method using transfer learning and deep convolutional neural network. *IEEE Journal of Selected Topics in Applied Earth Observations and Remote Sensing*, *13*, 1986–1995.

Luo, Y., Song, H., Wang, R., Deng, Y., Zhao, F., & Xu, Z. (2014). Arc FMCW SAR and applications in ground monitoring. *IEEE Transactions on Geoscience and Remote Sensing*, *52*(9), 5989–5998.

Miccinesi, L., Consumi, T., Beni, A., & Pieraccini, M. (2021a). W-band MIMO GB-SAR for Bridge Testing/Monitoring. *Electronics*, *10*(18), 2261.

Miccinesi, L., Consumi, T., Beni, A., & Pieraccini, M. (2021b). W-band MIMO GB-SAR for Bridge Testing/Monitoring. *Electronics*, *10*(18), 2261.

Miccinesi, L., & Pieraccini, M. (2020). Bridge Monitoring by a Monostatic/Bistatic Interferometric Radar Able to Retrieve the Dynamic 3D Displacement Vector. *IEEE Access*, *8*, 210339–210346. https://doi.org/10.1109/ACCESS.2020.3039381

Michel, C., & Keller, S. (2021). Advancing Ground-Based

Radar Processing for Bridge Infrastructure Monitoring. *Sensors*, *21*(6), 2172.

Monserrat, O., Crosetto, M., & Luzi, G. (2014). A review of ground-based SAR interferometry for deformation measurement. *ISPRS Journal of Photogrammetry and Remote Sensing*, *93*, 40–48.

Monti-Guarnieri, A., Falcone, P., d'Aria, D., & Giunta, G. (2018). 3D vibration estimation from ground-based radar. *Remote Sensing*, *10*(11), 1670.

Mugnai, F., Caporossi, P., & Mazzanti, P. (2022). Exploiting Image Assisted Total Station in Digital Image Correlation (DIC) displacement measurements: Insights from laboratory experiments. *Https://Doi.Org/10.1080/22797254.2021.2025153*, *55*(1), 115–128. https://doi.org/10.1080/22797254.2021.2025153

Mugnai, F., & Tarchi, D. (2022). Multiple-input multiple-output radar, ground-based MIMO SAR for ground deformation monitoring. *European Journal of Remote Sensing*, *55*(1), 604–621.

Omidalizarandi, M., Kargoll, B., Paffenholz, J. A., & Neumann, I. (2018). Accurate vision-based displacement and vibration analysis of bridge structures by means of an image-assisted total station: *Https://Doi.Org/10.1177/1687814018780052*, *10*(6), 2018. https://doi.org/10.1177/1687814018780052

Pepe, A., & Calò, F. (2017). A Review of Interferometric Synthetic Aperture RADAR (InSAR) Multi-Track Approaches for the Retrieval of Earth's Surface Displacements. *Applied Sciences 2017, Vol. 7, Page 1264*, *7*(12), 1264. https://doi.org/10.3390/APP7121264

Radman, A., Akhoondzadeh, M., & Hosseiny, B. (2021). Integrating InSAR and deep-learning for modeling and predicting subsidence over the adjacent area of Lake Urmia, Iran. *GIScience & Remote Sensing*, *58*(8), 1413–1433.

Rambour, C., Budillon, A., Johnsy, A. C., Denis, L., Tupin, F., & Schirinzi, G. (2020). From interferometric to tomographic SAR: A review of synthetic aperture radar tomography-processing techniques for scatterer unmixing in urban areas. *IEEE Geoscience and Remote Sensing Magazine*, *8*(2), 6–29.

Reigber, A., Scheiber, R., Jager, M., Prats-Iraola, P., Hajnsek, I., Jagdhuber, T., Papathanassiou, K. P., Nannini, M., Aguilera, E., Baumgartner, S., Horn, R., Nottensteiner, A., & Moreira, A. (2013). Very-High-Resolution Airborne Synthetic Aperture Radar Imaging: Signal Processing and Applications. *Proceedings of the IEEE*, *101*(3), 759–783. https://doi.org/10.1109/JPROC.2012.2220511

Sabato, A., Niezrecki, C., & Fortino, G. (2017). Wireless MEMS-Based Accelerometer Sensor Boards for Structural Vibration Monitoring: A Review. *IEEE Sensors Journal*, *17*(2), 226–235. https://doi.org/10.1109/JSEN.2016.2630008

Tarchi, D., Rudolf, H., Pieraccini, M., & Atzeni, C. (2000). Remote monitoring of buildings using a ground-based SAR: application to cultural heritage survey. *International Journal of Remote Sensing*, *21*(18), 3545–3551.

Wang, Y., Hong, W., Zhang, Y., Lin, Y., Li, Y., Bai, Z., Zhang, Q., Lv, S., Liu, H., & Song, Y. (2020). Ground-Based Differential Interferometry SAR: A Review. *IEEE Geoscience and Remote Sensing Magazine*, *8*(1), 43–70.

Wu, L., & Casciati, F. (2014). Local positioning systems versus structural monitoring: A review. *Structural Control and Health Monitoring*, *21*(9), 1209–1221. https://doi.org/10.1002/STC.1643

Zhang, G., Wu, Y., Zhao, W., & Zhang, J. (2020). Radar-based multipoint displacement measurements of a 1200-m-long suspension bridge. *ISPRS Journal of Photogrammetry and Remote Sensing*, *167*, 71–84.